Supporting Information

Green Low-cost User-friendly Elastomeric (GLUE) Microfluidics

Nicholas C. Speller [‡] *& Giorgio Gianini Morbioli,* [‡] *Michael E. Cato, Zachary A. Duca, and Amanda M. Stockton* [*]

School of Chemistry and Biochemistry, Georgia Institute of Technology, Atlanta, Georgia 30332, USA

[‡] *These authors contributed equally to this work*

***Corresponding author:** *Stockton, A.M.*

(astockto@gatech.edu)

Video S1: Operation of Proof-of-Concept devices fabricated using the GLUE method

Lowest-cost mold fabrication method – Blade coating

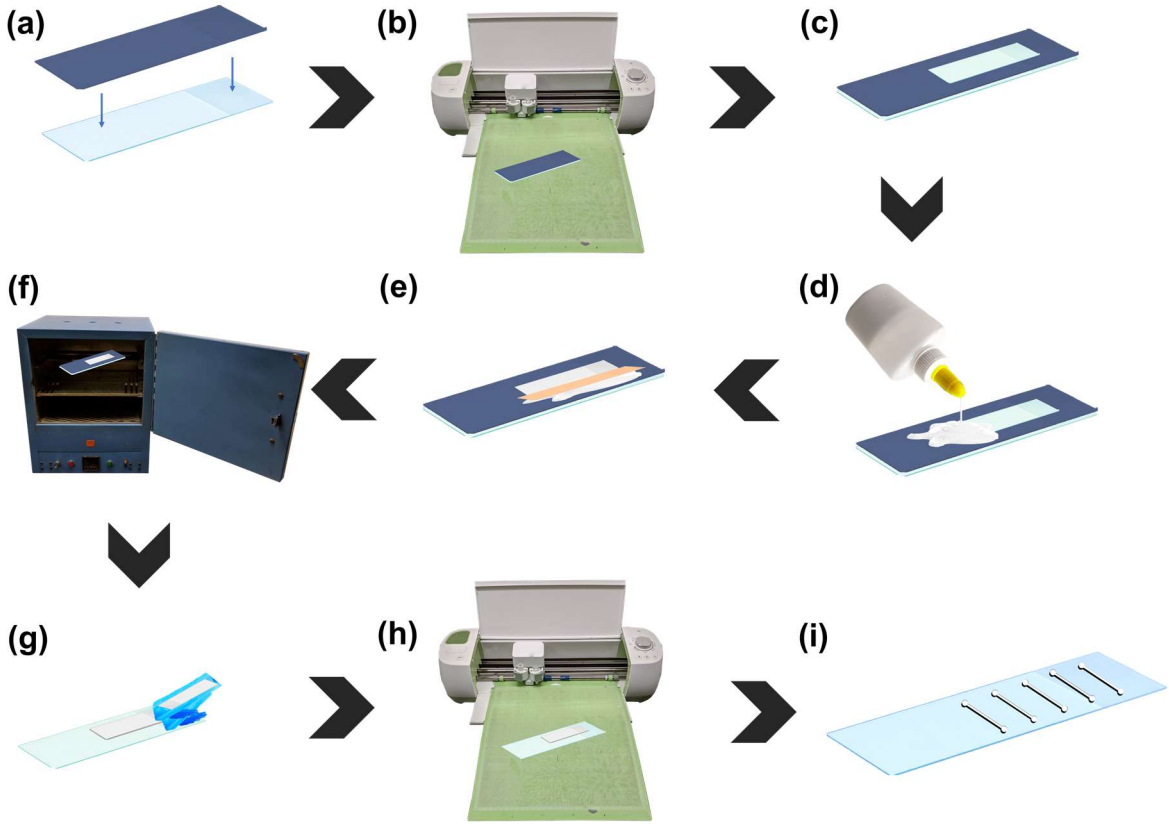

Figure S1. Step-by-step fabrication of PDMS-based microfluidic devices using the blade coating method. (a) PVC tape adhesion to a glass backing substrate. (b) Rectangle cutting on tape using a cutting plotter to create a glue reservoir. (c) Remove of the 'internal' rectangle, leaving the tape border on the backing substrate. (d) Water-soluble glue deposition on the edges of the tape of the mold. (e) Glue spreading onto the mold using a flat edge tool. (f) Glue curing in an oven. (g) Tape removal to expose the glue film. (h) CAD designs cutting on the glue film using a cutting plotter. (i) Glue mold.

Mold Cutting – Cutter Plotter

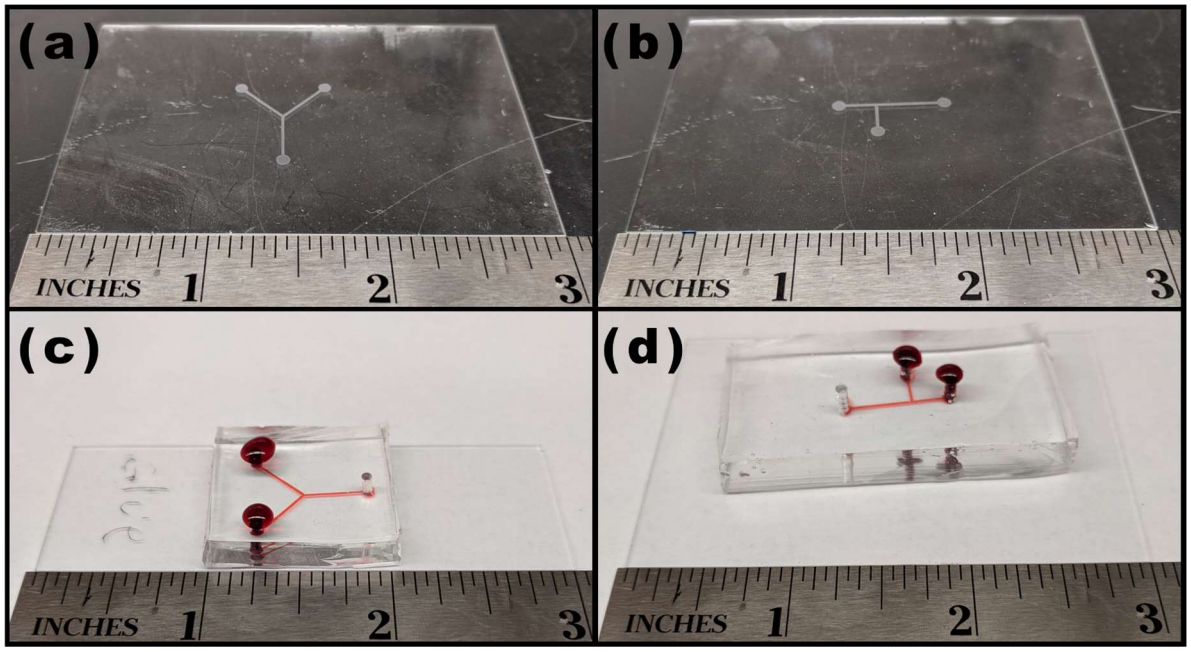

Figure S2. Proof-of-concept devices fabricated using the glue method and cut using the cutter plotter. (a) Glue mold of a Y-channel laminar flow generator (17.7 ± 0.4 µm tall, 415 ± 3 µm wide). (b) Glue mold of a T-droplet generator (18.3 ± 0.4 µm tall, 510 ± 20 µm wide). (c) PDMS-glass device of a Y-channel laminar flow generator filled with red dye. (d) PDMS-glass device of a T-droplet generator filled with red dye.

Proof-of-concept devices

3-valve normally open pneumatic pump fabrication

Briefly, the pump was designed in AutoCAD (Figure S3) and the fluidic layer was laser etched into a freshly prepared glue thin film on a PDMS substrate to create a glue mold on the PDMS substrate (Figure S4). A tape border was applied to the substrate and freshly degassed PDMS was squeegeed across the glue mold surface and cured during 30 min at 60 °C, creating a thin elastomer membrane (231 ± 2 µm),

as depicted in Figure S4. Subsequently, another glue thin film was prepared on the cured PDMS membrane layer as described previously, and the pattern was repeated to create the pneumatic layer (Figure S4). Degassed PDMS was cast over the pneumatic layer, cured, and fluidic access wells were cut into the pneumatic and fluidic layers. The complete, multilayer monolithic pneumatic pump was then sonicated as described in section 2.3.1 in the main manuscript to remove residual glue. Normally-open valves were chosen for this process to increase the rate of glue removal from the final device.

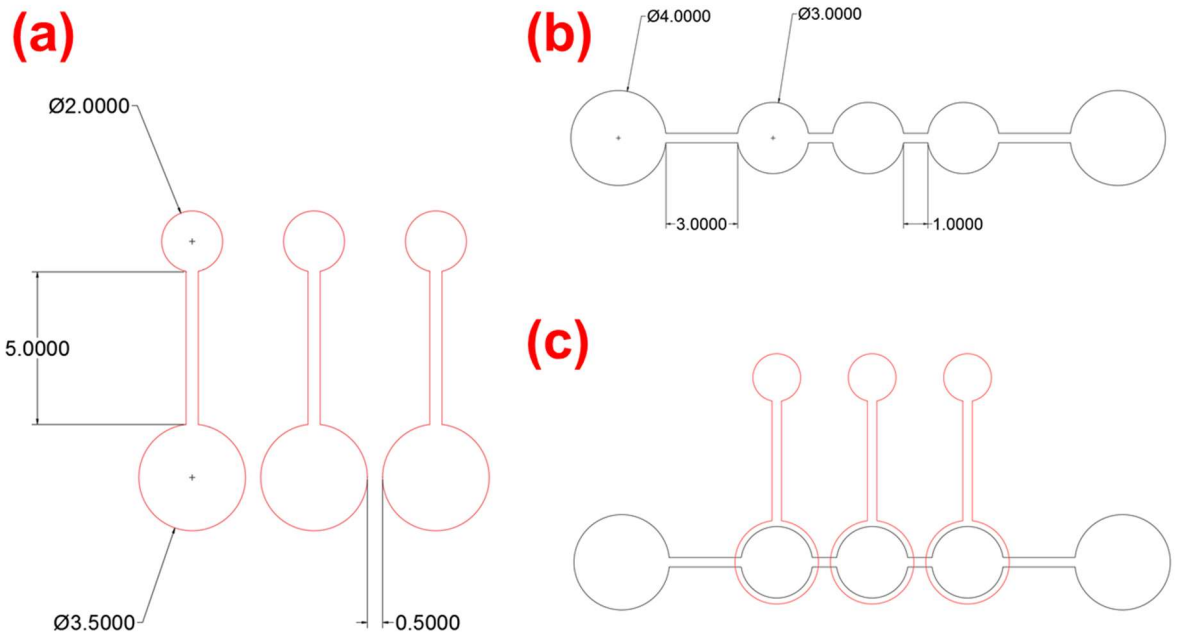

Figure S3. Design of a 3-valve normally open pneumatic pump. (a) Pneumatic layer design and dimensions. (b) Fluidic layer design and dimensions. (c) Layers aligned. All dimensions are in mm.

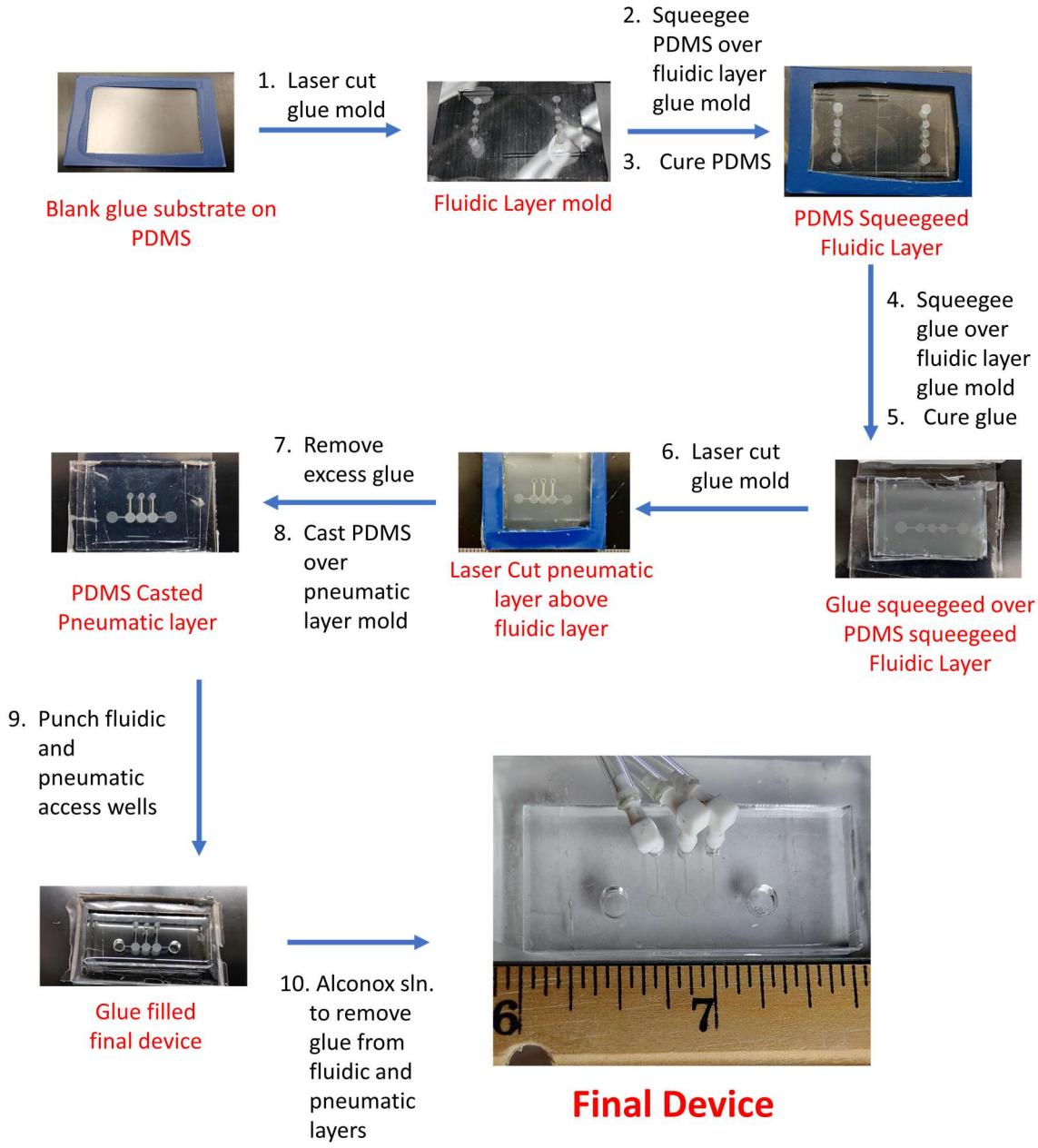

Figure S4. Fabrication steps of a 3-valve normally open pneumatic pump.

Pneumatic lifting gate microfluidic processor fabrication

Briefly, the pump was designed in AutoCAD (Figure S5), and a glue thin-film was freshly prepared on a glass substrate (Figure S6). The fluidic layer pattern was vector cut (20% PWR 85% SPD) from the glue thin film while lifting gate feature molds were raster etched (12.5% PWR 40% SPD) into the valve regions of the fluidic layer (Figure S6), all during the same laser cutting step. A tape border was applied to the substrate and freshly degassed PDMS was squeegeed across the glue mold surface and cured (Figure S6). This created a thin membrane layer (231 ± 2 μm) containing the fluidic channels and perfectly aligned 3-dimensional lifting gate features as depicted in Figure S6, in a single, simple reproducible step. Another glue thin-film on a glass substrate was prepared and the pattern for the pneumatic layer was laser cut and the excess from the glue film was removed. PDMS was cast over the pneumatic layer mold, cured and fluidic and pneumatic access wells were cut using a biopsy punch. The pneumatic layer was aligned by eye and bonded to the thin film fluidic layer prepared in the previous step. Then, fluidic access wells were cut into the film layer. The monolith containing the pneumatic layer and thin film layer was then removed, and a small drop of glue was applied to each of the lifting gate features and cured to prevent bonding of the lifting gate features in the final step. Finally, the PDMS monolith was plasma bonded to a glass slide to seal the fluidic layer yielding the final device. Alconox solution was cycled through the device using the mixing routine to remove excess glue from the lifting gate features.

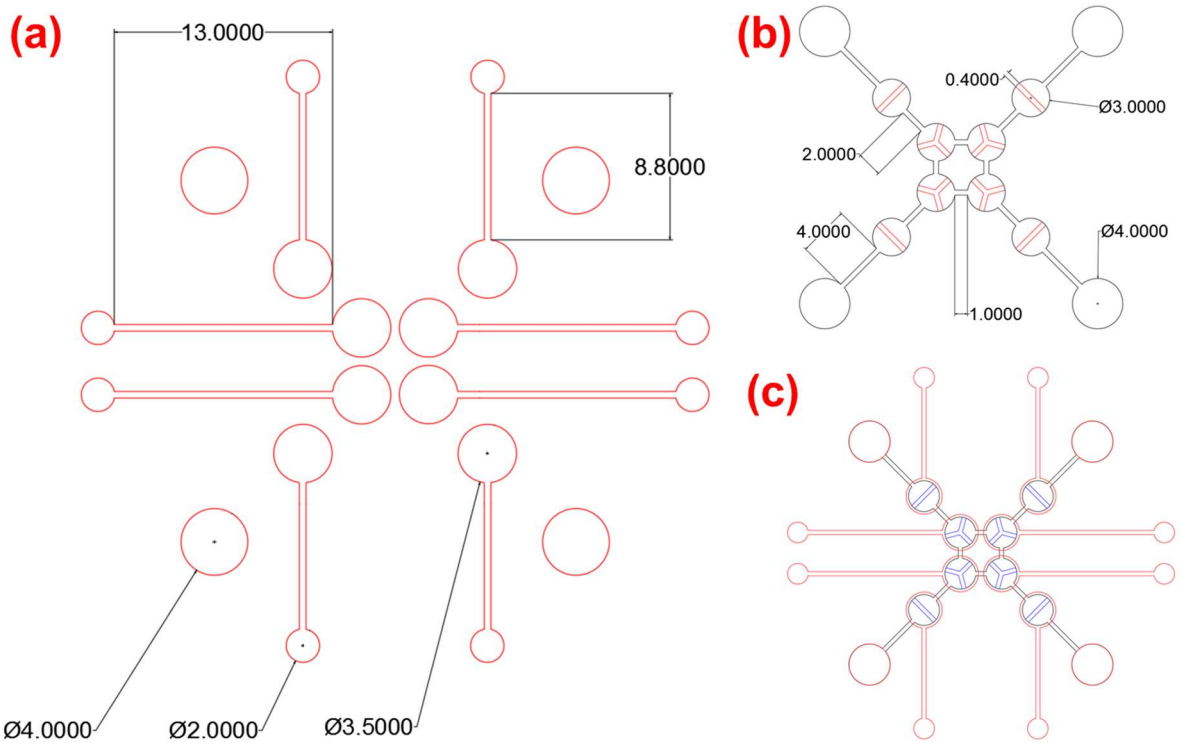

Figure S5. Design of a pneumatic lifting gate microfluidic processor. (a) Pneumatic layer design and dimensions. (b) Fluidic layer design and dimensions. (c) Layers aligned. All dimensions are in mm.

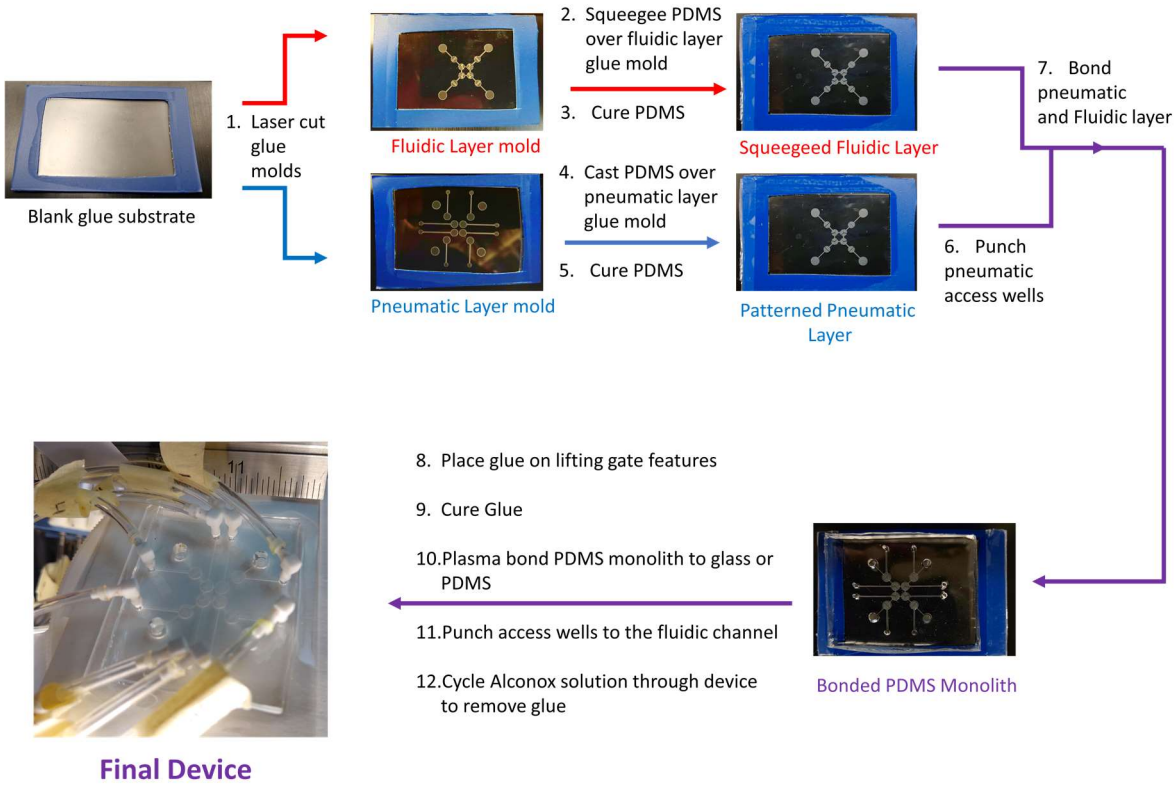

Figure S6. Fabrication steps of a pneumatic lifting gate microfluidic processor.

Device testing

Microchip working pressure testing

To test the mechanical resistance of scaffolded PDMS devices, glue molds were fabricated on freshly cast PDMS slabs (4 mm thick) using the blade coating method using 3 layers of PVC tape. CAD designs were cut into the glue molds using the laser cutter, and degassed PDMS was cast onto these molds. After curing (conventional oven, 3 h, 60 ^{o}C), PDMS devices were sonicated with a warm soap solution to remove the glue from the channels, as described in Section 2.3 in the main manuscript. Microchannels were designed to be 1-cm long and 600 µm wide.

Using a syringe pump (kd Scientific, Legato® 180, Holliston, MA), DI water was infused through the microchips with different flow rates (100 µL min^{-1}, 200 µL min^{-1}, 300 µL min^{-1}, 400 µL min^{-1}, 500 µL min^{-1}, 750 µL min^{-1}, 1 mL min^{-1}, 5 mL min^{-1}, 10 mL min^{-1} and 14.2 mL min^{-1}), for 30 s per rate. A pressure sensor (LabSmith, 0800 uPS Pressure Sensor, Livermore, CA) was placed at the beginning of the microchannel, and it was connected to a microfluidic automation datalogging system (LabSmith, uProcess™ System, Livermore, CA) connected to a computer. The pressure testing system is shown in Figure S7.

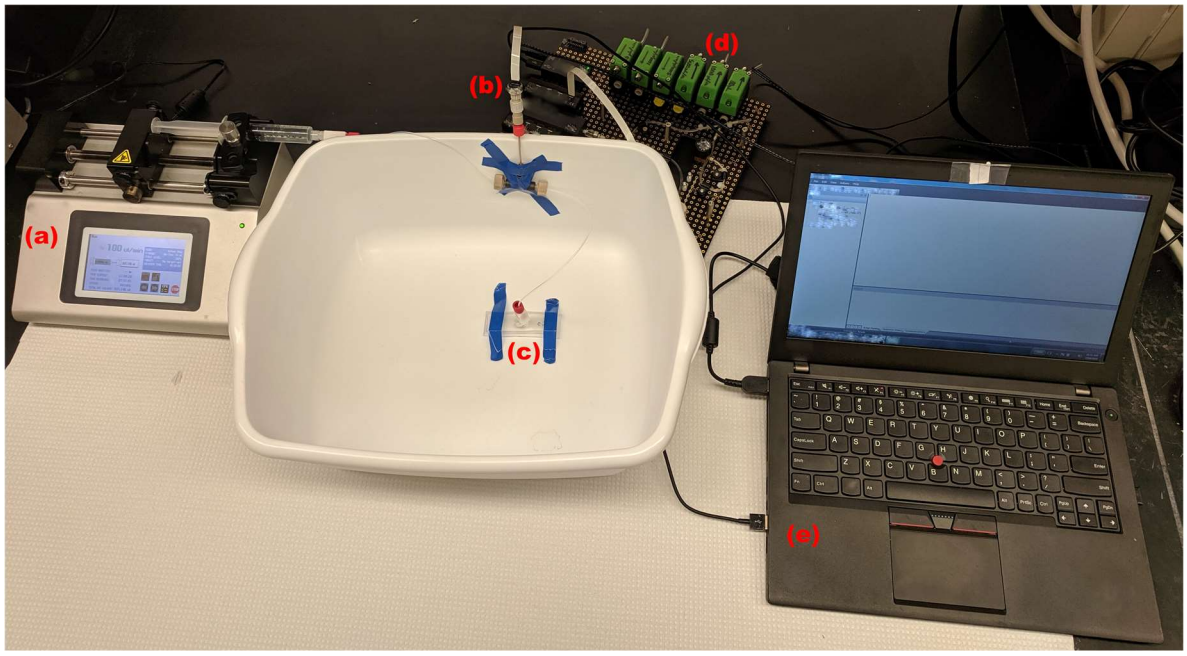

Figure S7. Photograph of the experimental setup for microchip working pressure testing. (a) Syringe pump (kd Scientific, Legato® 180, Holliston, MA). (b) Fluidic pressure sensor (LabSmith, 0800 uPS Pressure Sensor, Livermore, CA). (c) PDMS-PDMS microchip. (d) Microfluidic automation system (LabSmith, uProcess™ System, Livermore, CA). (e) Computer.

Y-channel laminar flow generator

Y-channel devices were designed using AutoCAD and were fabricated according to the procedure described in Section 2.3, using the sticker cutter to cut the glue films (Figure S2a and c). One inlet was infused using a black dye solution in DI water, and the second inlet was infused with DI water. Two syringe pumps (kd Scientific, Legato® 180, Holliston, MA) were used to provide different flow rates for each inlet of the Y-channel device (50 μL min^{-1}, 100 μL min^{-1} and 200 μL min^{-1}). The pumping of solutions was recorded using a digital microscope (AD-413MT-FVW Series Digital Microscope, DinoLite, Torrance, CA).

Droplet generator

A T-droplet generator device was designed using AutoCAD and was fabricated according to the procedure described in Section 2.3, using the sticker cutter to cut the glue films (Figure S2b and d). Using a syringe pump, a black dye testing solution in DI water was infused at one inlet of the device, with a rate of 22 μL min^{-1}, and soybean oil was infused at the other inlet, with a rate of 25 μL min^{-1}. The droplet generation was recorded using a digital microscope.

3-valve normally open pneumatic pump

A LabView program was used to actuate a bank of solenoid valves, which were connected to a vacuum and a N_2 pressure line.[1] Each valve of the pneumatic pump was connected to a solenoid valve of the bank and was actuated individually. Different wait times for each step in the pumping routine were used (25 ms, 50 ms,

100 ms, 150 ms and 200 ms), yielding different pumping rates. The pumping routine is depicted in Figure S8. A blue dye solution in DI water was used as the testing solution to enable visualization. The pumping of solutions was timed and recorded using a digital microscope.

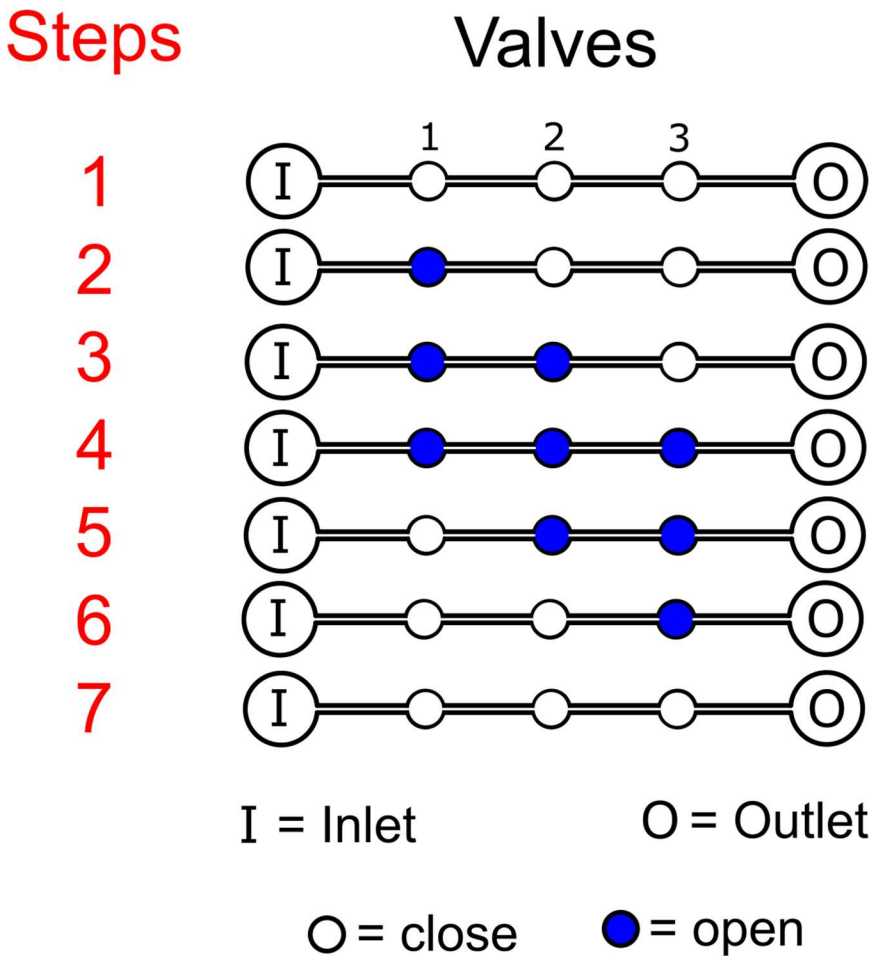

Figure S8. Valve opening and closing routine of the 3-valve normally open pneumatic pump.

Pneumatic lifting gate microfluidic processor

A custom LabView program was used to actuate the solenoid valves [1], a blue dye solution in one inlet and a yellow dye solution in a second inlet were combined using the microfluidic processor, generating a green dye mixture at the outlet. The dye mixing routine is shown in Figure S9, and the opening and closing valve sequence is depicted in Figure S10. The valves of the processor were cleaned using DI water (Figure S11), which was added to a third inlet of the processor. The opening and closing valve sequence are depicted in Figure S12. Figure S13 shows still frame pictures of the cleaning process. The dye mixture and cleaning routines were recorded using a digital microscope.

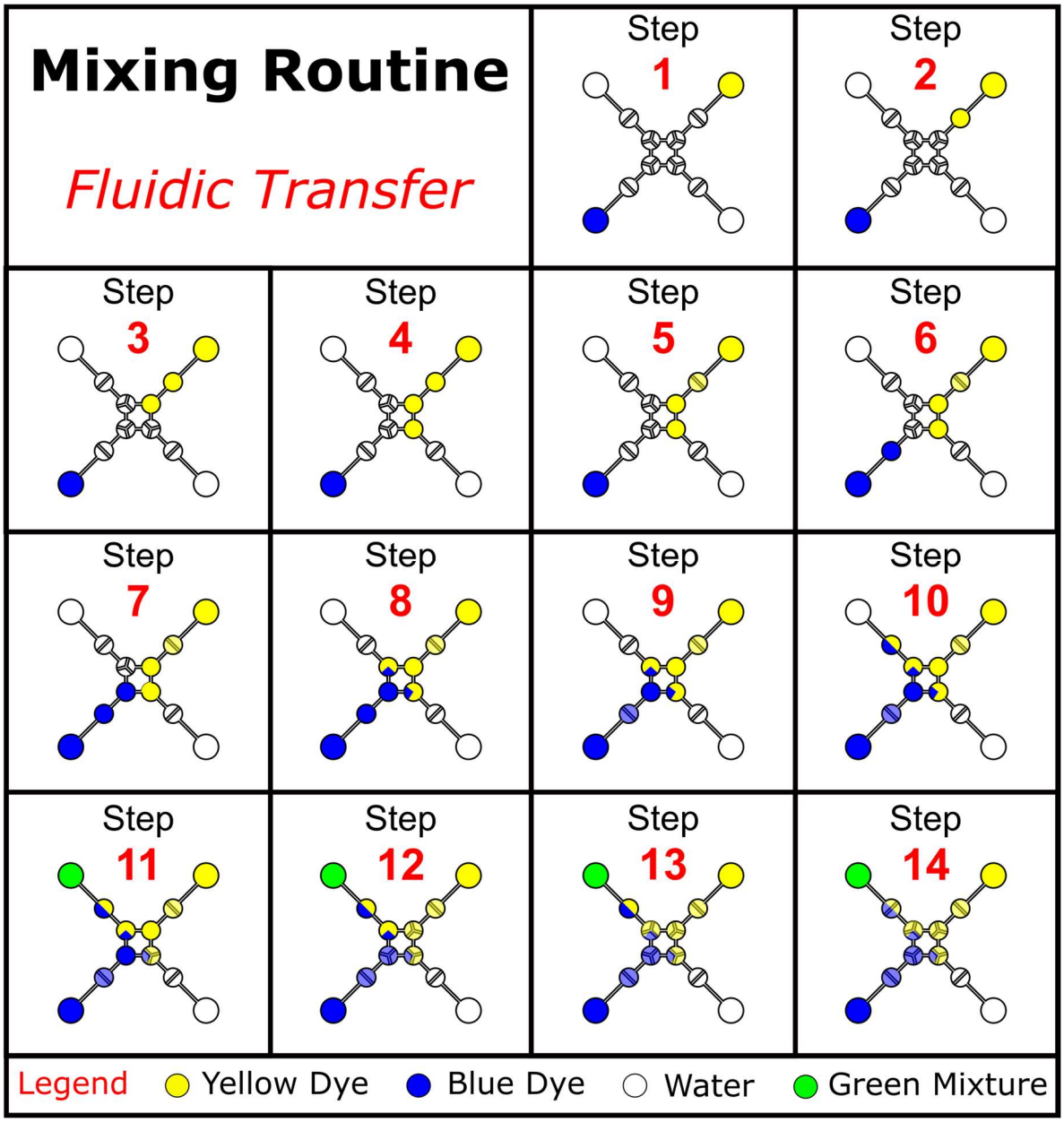

Figure S9. Schematics of the dye mixing routine used in the fluidic processor.

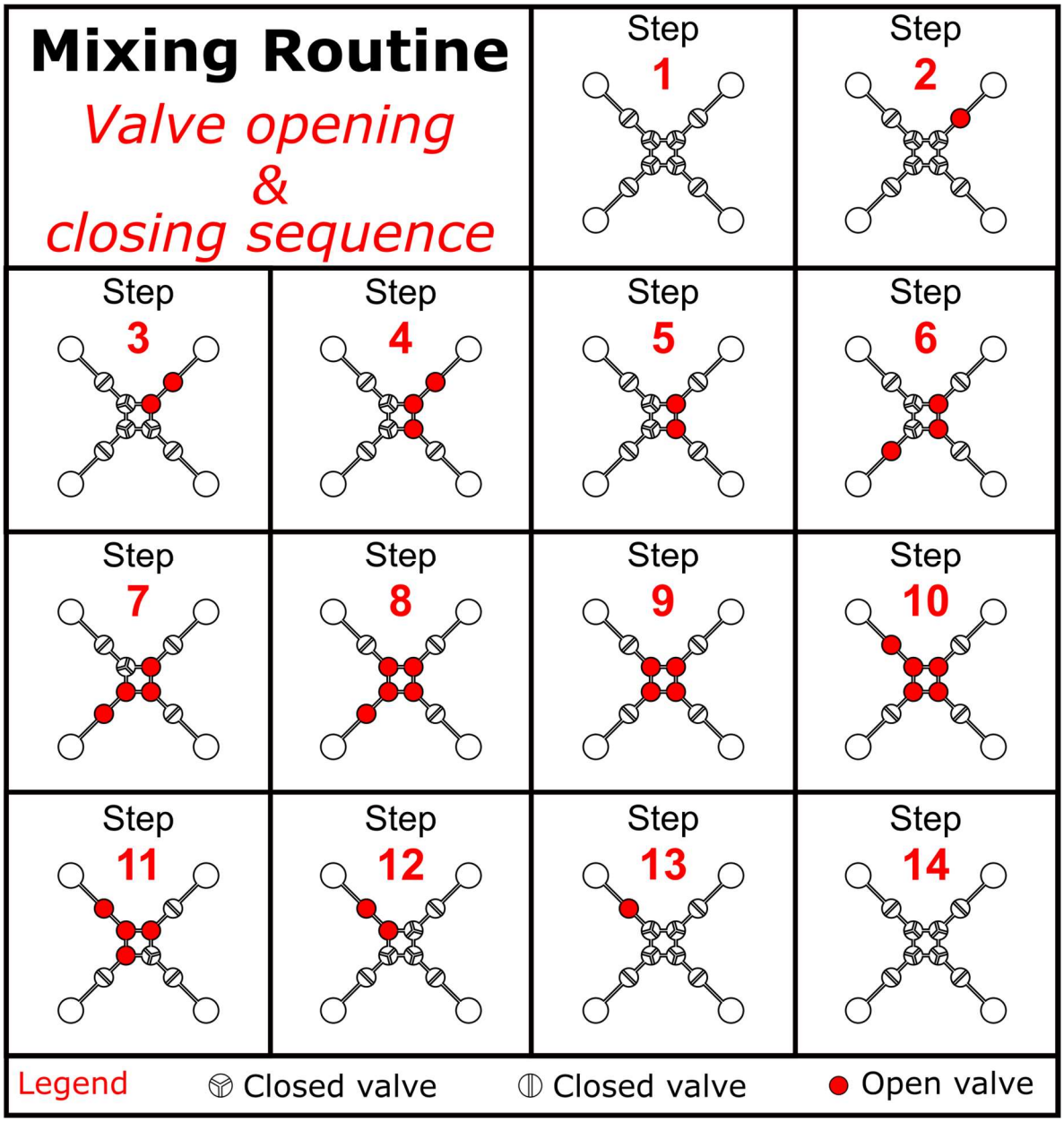

Figure S10. Schematics of the opening and closing valve sequence used for the mixing routine depicted in Figure S9.

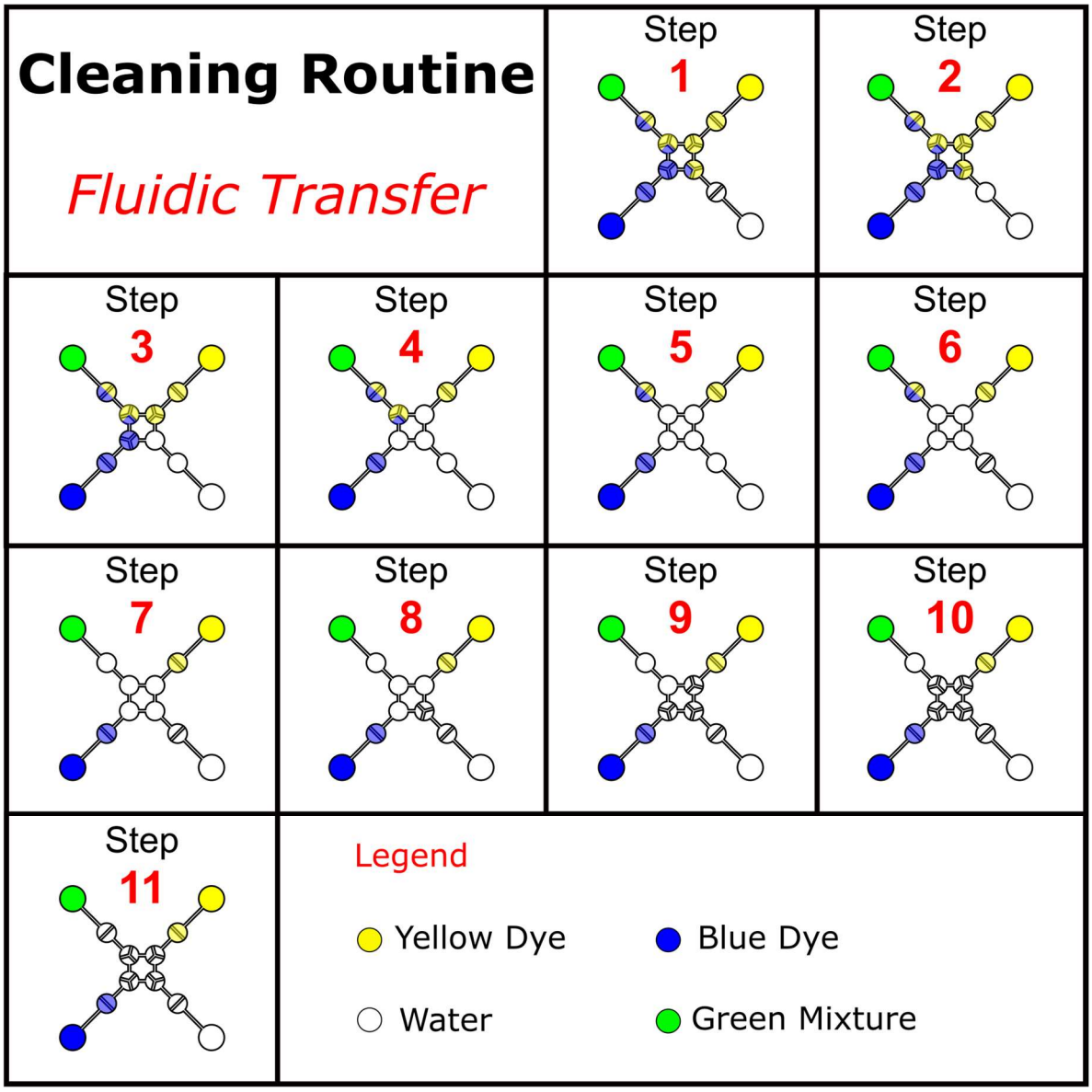

Figure S11. Schematics of the cleaning routine used in the fluidic processor.

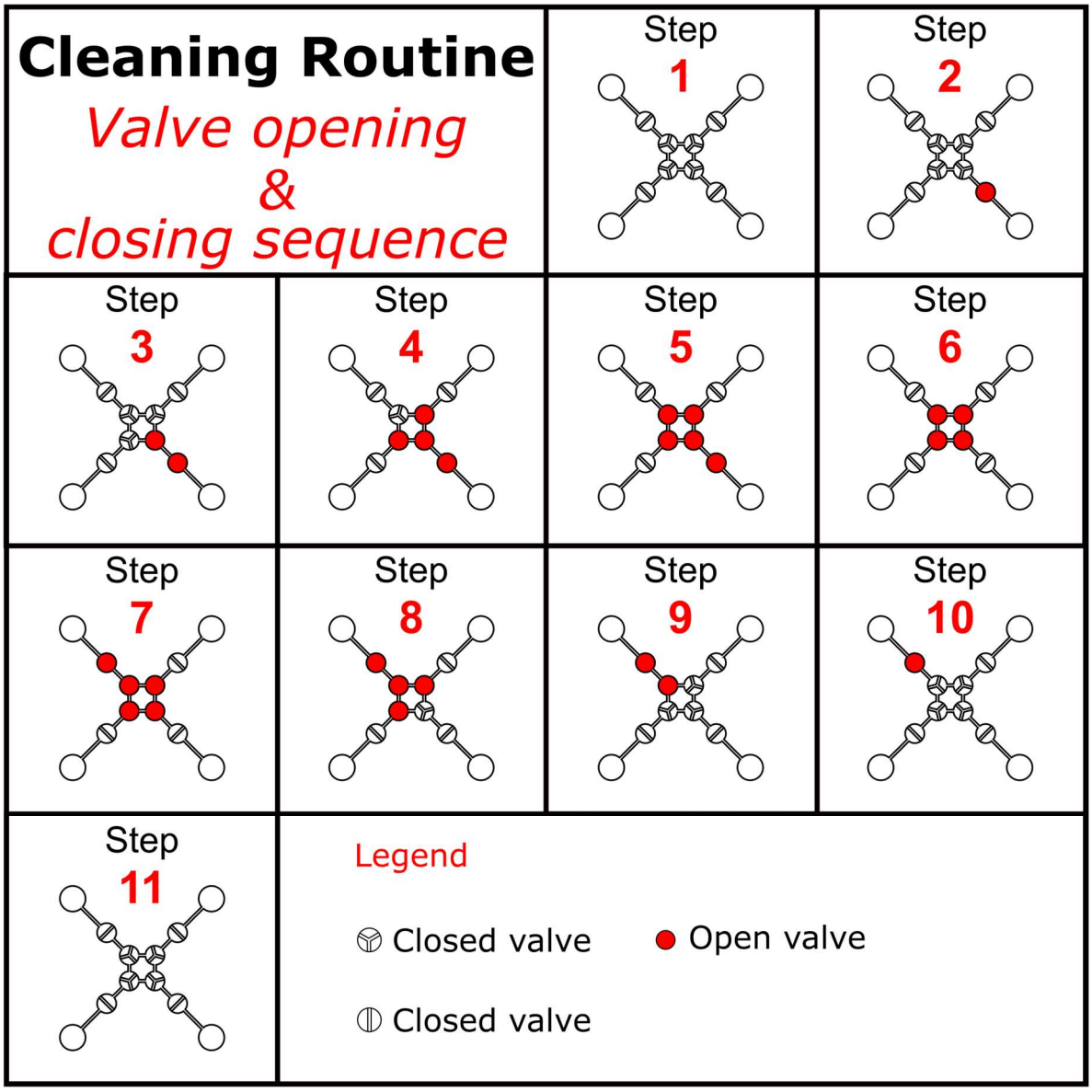

Figure S12. Schematics of the opening and closing valve sequence used for the cleaning routine depicted in Figure S11.

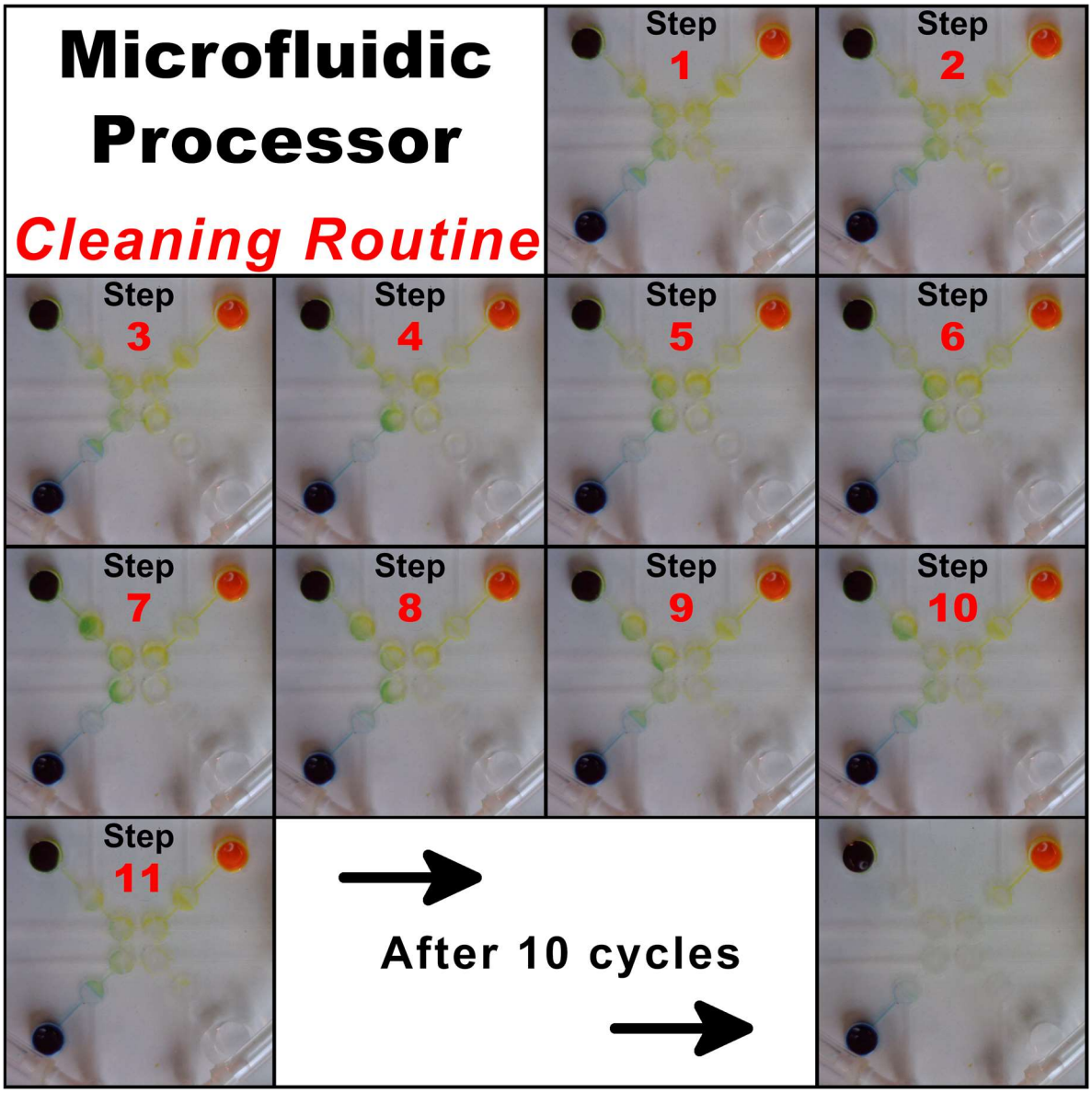

Figure S13. 2x2 microfluidic processor used to perform a cleaning routine, after mixing the dyes. Water in a fourth inlet is pumped through all the processor valves, cleaning the residues of dye present from the mixing protocol. After 10 cycles, the processor valves are clean, and can be used for other protocols.

Glue film composition

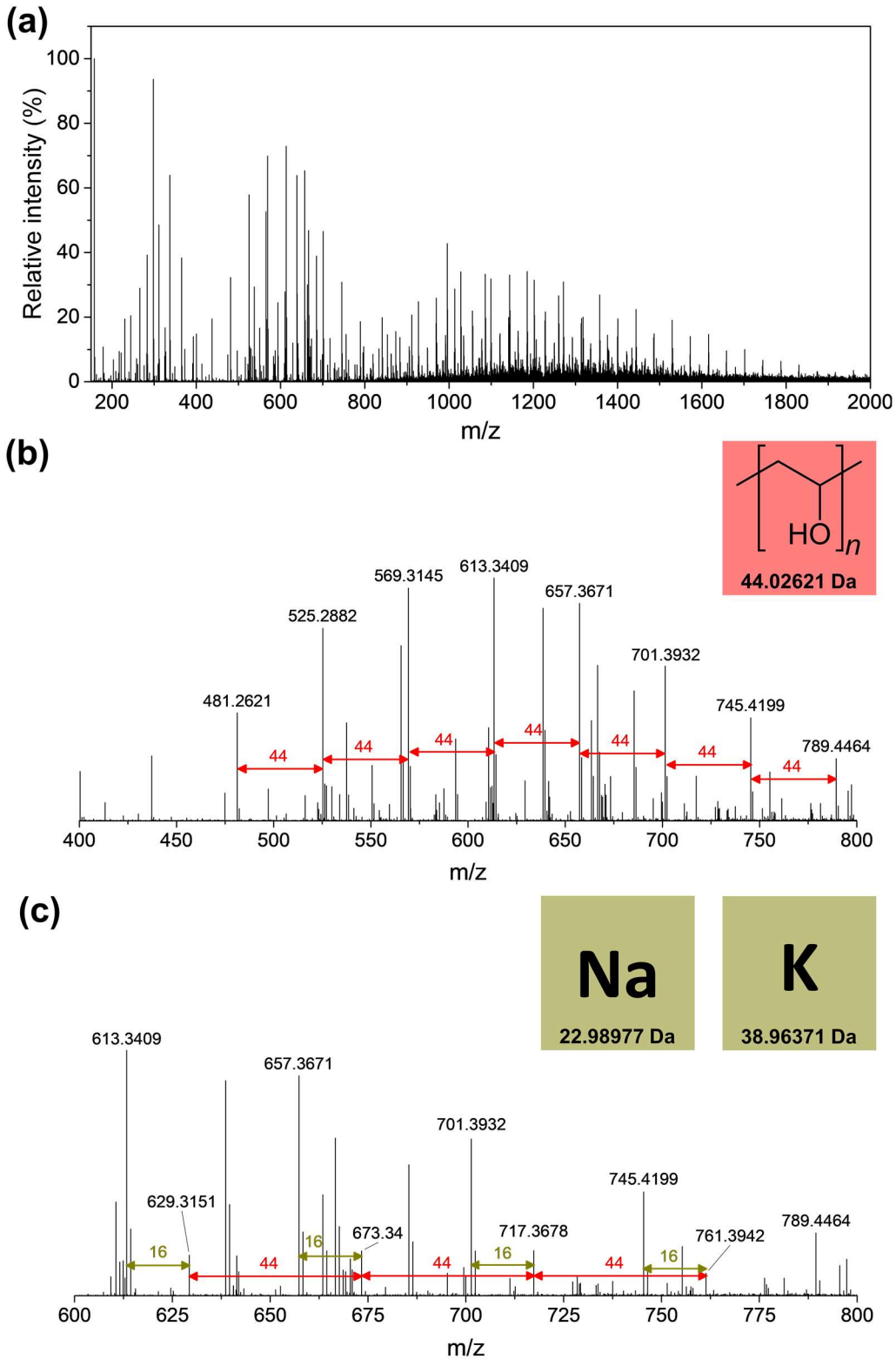

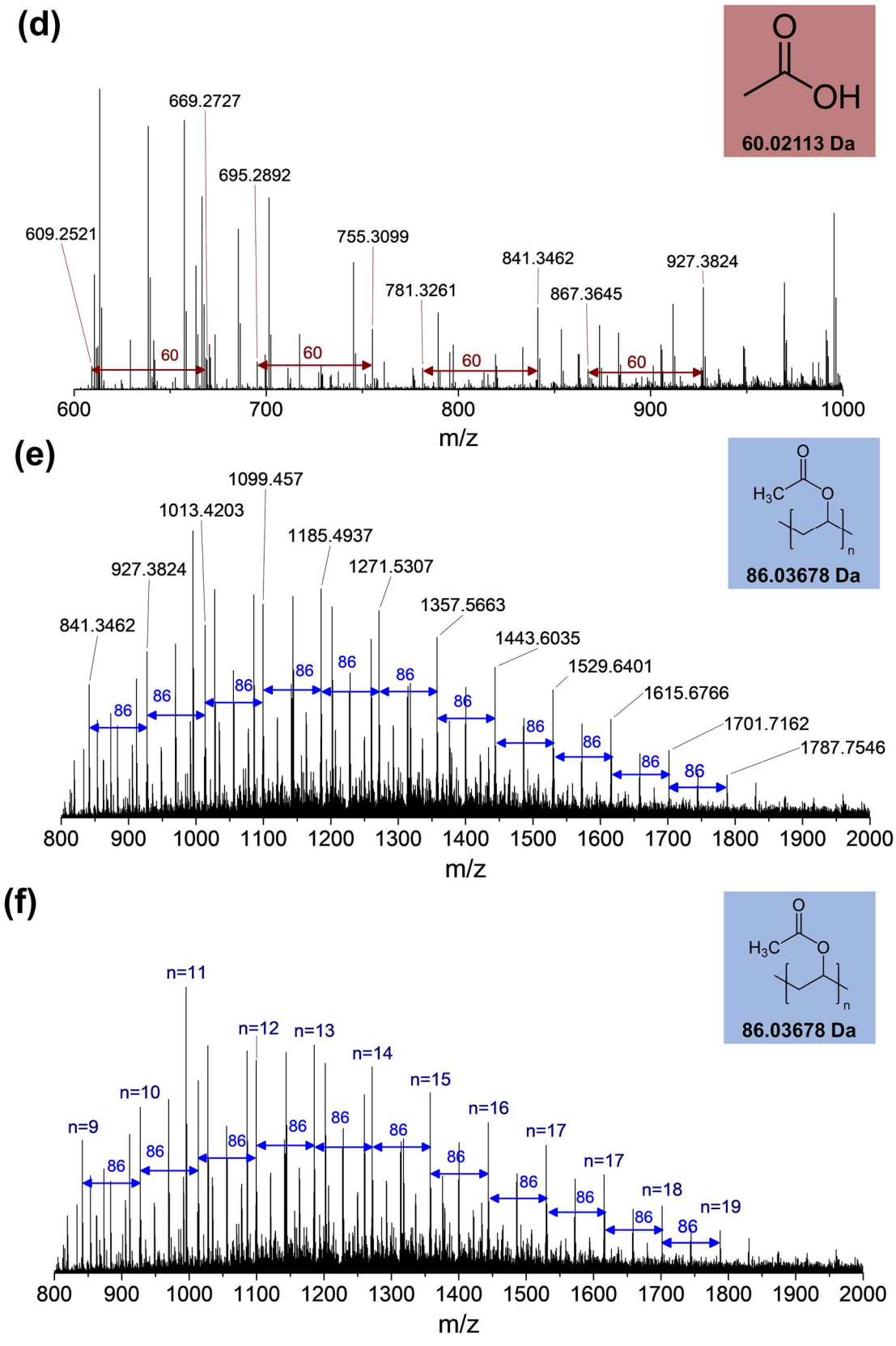
(d)
O
OH
60.02113 Da
669.2727
695.2892
609.2521
755.3099
841.3462
927.3824
781.3261
867.3645
60
60
60
60
600
700
800
900
1000
m/z
(e)
1099.457
1013.4203
1185.4937
927.3824
1271.5307
1357.5663
841.3462
1443.6035
1529.6401
1615.6766
1701.7162
1787.7546
86.03678 Da
86
800
900
1000
1100
1200
1300
1400
1500
1600
1700
1800
1900
2000
m/z
(f)
n=11
n=12
n=13
n=14
n=15
n=16
n=17
n=10
n=9
n=17
n=18
n=19
86.03678 Da
86
800
900
1000
1100
1200
1300
1400
1500
1600
1700
1800
1900
2000
m/z

Figure S14. ESI-orbitrap mass spectrum of white glue. (a) Mass spectrum with m/z ranging from 150 to 2000 Th. (b) Expanded region of the mass spectrum (m/z from 400 to 800 Th). The difference between peaks is annotated with red arrows and corresponds to the mass of a vinyl alcohol monomer (44 Da). (c) Expanded region of the mass spectrum (m/z from 600 to 800 Th). The difference between peaks (16 Da) is annotated with gold arrows and corresponds to the mass difference between sodium (23 Da) and potassium (39 Da) adducts of polymers with the same chain size. (d) The loss of acetic acid (60 Da) from PVAc polymeric chains is annotated with maroon arrows between peaks. (e) Expanded region of the mass spectrum (m/z from 800 to 2000 Th). The difference between peaks is annotated with blue arrows and corresponds to the mass of a vinyl acetate monomer (86 Da). (f) Same region from (e), with peaks annotated with their degree of polymerization (denotated as n). Peaks in all spectra are marked with their m/z values, if not stated otherwise. Sample preparation: a white glue sample (0.5 g) was dissolved in 1 mL of a solution of H_2O : Acetonitrile (50:50 $_{(V/V)}$) with 0.1% $_{(V/V)}$ of formic acid, and subsequently diluted with methanol (100-fold). Analysis was performed using a Thermo Scientific LTQ Orbitrap XL mass spectrometer, with an electrospray ion source. Analysis conditions: Positive ion mode; Direct infusion with methanol, syringe pump flow rate = 8 μL min^{-1}; ESI source: Spray Voltage = 5 kV, Capillary Voltage = 80.03 V, Capillary Temperature = 235.06 °C.

Table S1: Compositional analysis of PVAc oligomers represented in Figure S14f

n	Compositional Assignment	Experimental mass (Da)	Theoretical Data (Da)	ppm error
9	$[(C_2H_5(C_4H_6O_2)_9CH_3)Na]^+$	841.3462	841.3828	43
10	$[(C_2H_5(C_4H_6O_2)_{10}CH_3)Na]^+$	927.3824	927.4196	40
11	$[(C_2H_5(C_4H_6O_2)_{11}CH_3)Na]^+$	1013.4203	1013.4564	36
12	$[(C_2H_5(C_4H_6O_2)_{12}CH_3)Na]^+$	1099.4570	1099.4932	33
13	$[(C_2H_5(C_4H_6O_2)_{13}CH_3)Na]^+$	1185.4937	1185.5300	31
14	$[(C_2H_5(C_4H_6O_2)_{14}CH_3)Na]^+$	1271.5307	1271.5667	28
15	$[(C_2H_5(C_4H_6O_2)_{15}CH_3)Na]^+$	1357.5663	1357.6035	27
16	$[(C_2H_5(C_4H_6O_2)_{16}CH_3)Na]^+$	1443.6035	1443.6403	25
17	$[(C_2H_5(C_4H_6O_2)_{17}CH_3)Na]^+$	1529.6401	1529.6771	24
18	$[(C_2H_5(C_4H_6O_2)_{18}CH_3)Na]^+$	1615.6766	1615.7139	23
19	$[(C_2H_5(C_4H_6O_2)_{19}CH_3)Na]^+$	1701.7162	1701.7506	20
20	$[(C_2H_5(C_4H_6O_2)_{20}CH_3)Na]^+$	1787.7546	1787.7874	18

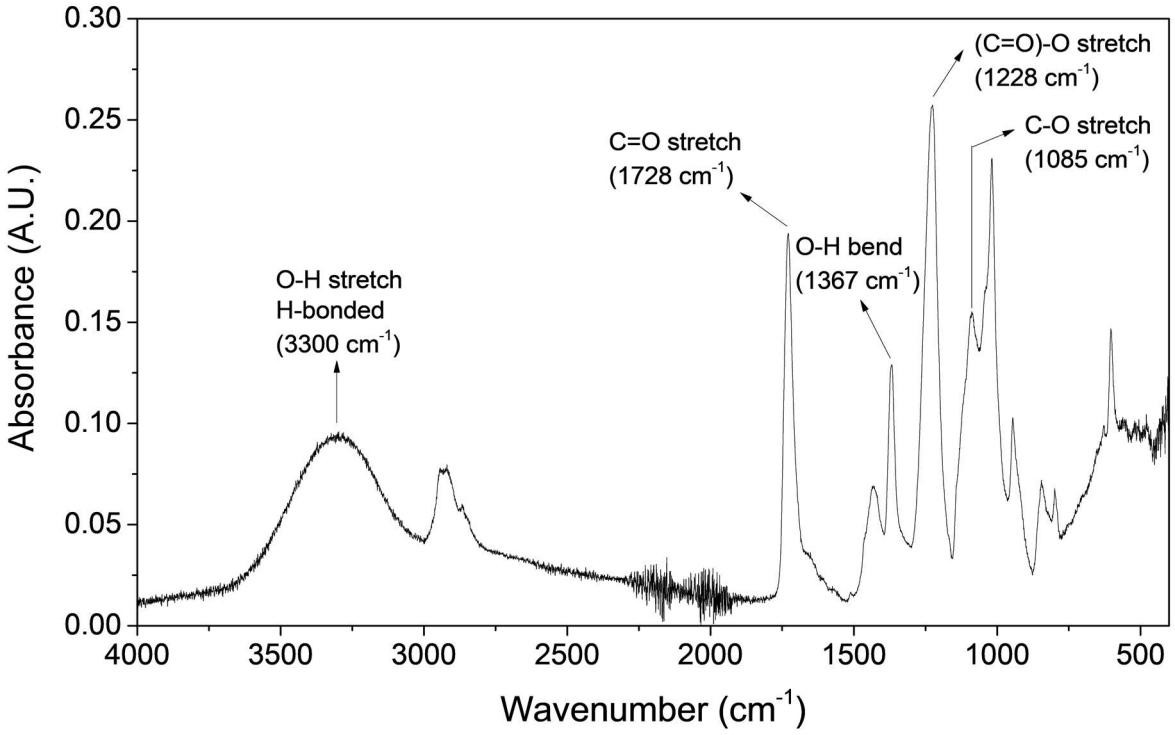

Figure S15. ATR-FTIR spectrum of a dried glue film. The polymeric film is composed of poly (vinyl acetate), evidenced by the C=O and (C=O)-O stretches, and poly (vinyl alcohol), evidenced by the H-bonded O-H stretch and O-H bend. Analysis was performed using a Thermo Nicolet Nexus 4700 FT-IR spectrometer with a diamond crystal horizontal ATR cell in the reflectance mode. Scan settings are: resolution 1.0 cm^{-1}, 64 scans, range: 400 to 4000 cm^{-1}.

Laser cutter characterization

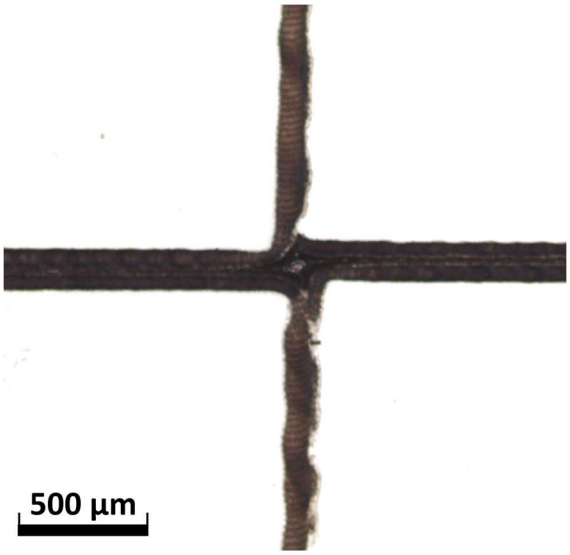

Figure S16. Confocal laser micrograph of a glue mold cut into a cross-shape with a laser cutter. Channel width was designed to 100 µm. The glue was totally ablated from the substrate in the vertical orientation (horizontal belt mechanism) because the nominal width was designed with a size smaller than the laser cutter offset.

Table S2: Statistical z-test comparing the line width of molds cut in vertical and horizontal orientations with the laser cutter, using the regression parameters from Table S3. Both cutting orientations did not show a statistically significant difference for nominal lines over 200 µm with a confidence interval of 95% ($p_{(z)}>p_{(0.05)}$)

	Calculated z	p(z)	p(0.05)	p(z)>p(0.05)?	Reject Null Hypothesis?
Intercept	1.149	0.8749	0.05	True	No
Slope	-0.09732	0.4602	0.05	True	No

Table S3: Comparison between the linear regressions of the vertical cutting orientation and horizontal cutting orientation, with a confidence interval (C.I.) of 95%*

	Vertical		Horizontal	
r^2	0.999		0.996	
Confidence interval	2.5%	97.5%	2.5%	97.5%
Intercept / µm	-144	-128	-170	-130
Slope / A.U.	1.00	1.02	1.00	1.04

* Obtained using Origin 2016 Software.

Equation correlating spin coating speed and film thickness

$$\delta \propto \frac{1}{\sqrt{\omega}} \quad \text{(S1)}$$

δ is the film thickness;

ω is the rotational speed.

Table S4: White glue viscosity measurements

Measurement	Temperature (°C)	Viscosity (cP)	Flow rate (µL min^{-1})	Shear rate (s^{-1})	Shear stress (Pa)	Volume (µL)	r^2
1	22.89	2862	59.4	62.8	179.73	17.1	1
2	22.88	2852	59.4	62.8	179.09	19.0	1
3	22.86	2810	59.4	62.8	176.45	63.5	1
4	22.92	2797	56.0	59.2	165.63	13.8	1
5	22.92	2862	56.0	59.2	169.45	13.8	1
6	22.91	2934	56.0	59.2	173.73	16.2	1
Average	22.90	2853	58	61	174	24	1
Std. dev.	0.02	50	2	2	6	20	0

Analysis was performed using a RheoSense microVISC Viscometer/Rheometer-on-a-Chip.

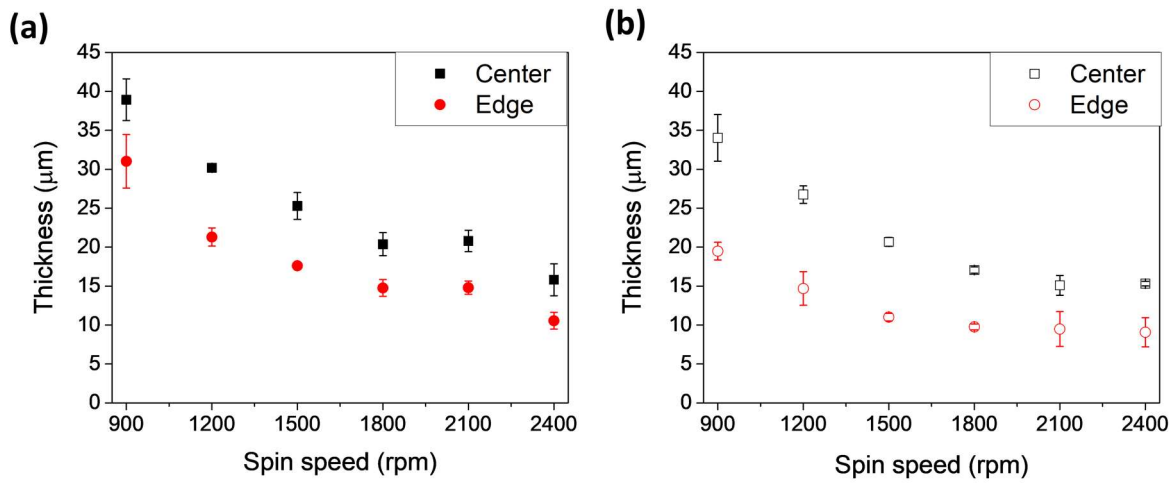

Figure S17. Characterization of glue molds. (a) Glue mold film thicknesses spun at different speeds in the spin coater on glass substrates. (b) Glue mold film thicknesses spun at different speeds in the spin coater on PDMS substrates. The values in all plots represent the average of 3 measurements ± 1 standard deviation.

Table S5: *t*-tests comparing the height of glue molds and the height of PDMS channels cast on its respective glue mold (C.I. 95%). There is no significant statistical difference between the height of glue molds and the PDMS channels cast on its respective mold ($t_{calc}<t_{crit}$)

	1 Spin		2 Spins		3 Spins	
	Mold	*PDMS*	*Mold*	*PDMS*	*Mold*	*PDMS*
Average	22.55	21.16	59.86	60.01	103.01	103.84
Variance	2.35	0.55	7.50	5.69	22.27	14.99
Number of observations	3	3	3	3	3	3
Pearson correlation	1.45		6.59		18.63	
Hypothesis test for difference of means	0		0		0	
df	4		4		4	
t calc	1.411		-0.073		-0.235	
P(T<=t) one-tailed	0.115		0.472		0.413	
t crit one-tailed	2.132		2.132		2.132	
P(T<=t) two-tailed	0.231		0.945		0.825	
t crit two-tailed	2.776		2.776		2.776	

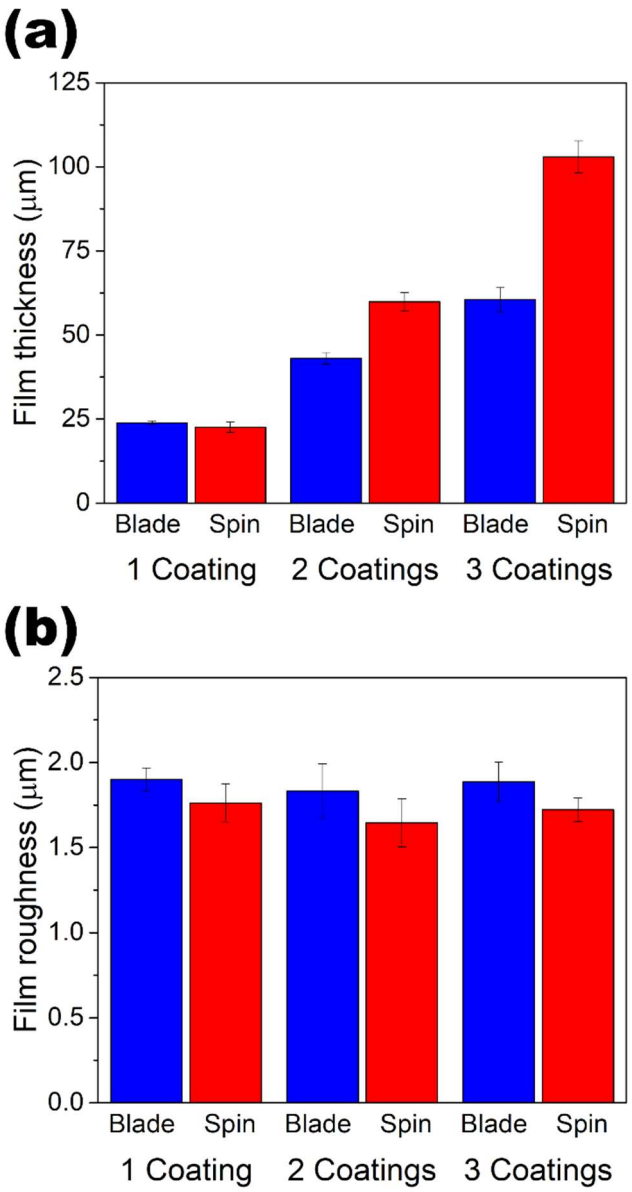

Figure S18. Characterization of glue molds fabricated using the two methods. (a) Film thickness of glue molds created using multiple layers of tape via the blade method and via multiple depositions using the spin coating method. (b) Glue thin film surface roughness (root-mean-square of laser confocal profiles) of films made via both methods. The values in all plots represent the average of 3 measurements ± 1 standard deviation.

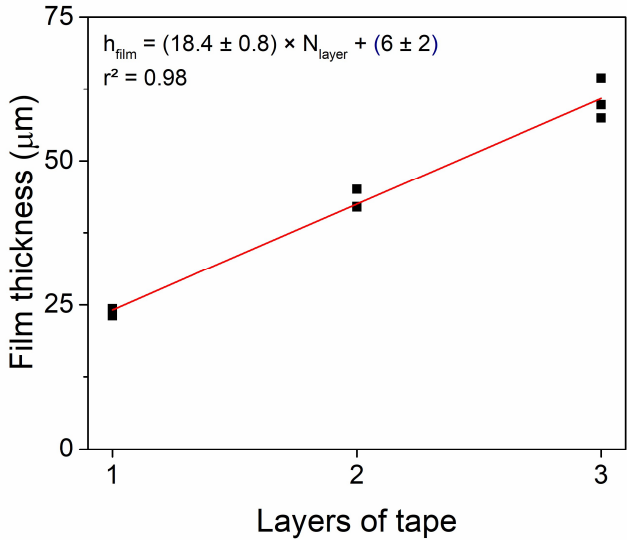

Figure S19. Variation of glue mold thickness with the number of layers of tape used in the blade coating method. For each additional layer of tape added, the height of the glue mold increases 18.4 ± 0.8 μm, accordingly to the best fit regression.

Table S6: One-way ANOVA test comparing the surface roughness of glue molds fabricated with multiple layers of PVC tape or multiple spins of glue. There is no statistically significant differences between glue molds fabricated using 1, 2 or 3 layers of PVC tape ($F_{calc}<F_{crit}$); between glue molds fabricated with 1,2,or 3 spins ($F_{calc}<F_{crit}$); or between blade coating and spin coating methods ($F_{calc}<F_{crit}$)

Raw data					
Surface roughness (root mean square (RMS)) (μm)					
1 Layer	2 Layers	3 Layers	1 Spin	2 Spins	3 Spins
1.911	1.764	2.019	1.721	1.657	1.779
1.962	1.717	1.802	1.888	1.497	1.644
1.83	2.015	1.837	1.677	1.78	1.744

One-way ANOVA – Surface roughness of blade coating using multiple layers of tape

Source of Variation	*SS*	*df*	*MS*	*F*	*P-value*	*F crit*
Between groups	0.00790	2	0.004	0.271	0.771	5.143
Within groups	0.08735	6	0.015			
Total	0.09525	8				

One-way ANOVA – Surface roughness of spin coating with multiple spins of glue

Source of Variation	*SS*	*df*	*MS*	*F*	*P-value*	*F crit*
Between groups	0.0214	2	0.011	0.856	0.471	5.143
Within groups	0.0749	6	0.0125			
Total	0.0962	8				

One-way ANOVA – Surface roughness of blade coating and spin coating

Source of Variation	*SS*	*df*	*MS*	*F*	*P-value*	*F crit*
Between groups	0.1493	5	0.030	2.209	0.121	3.106
Within groups	0.1622	12	0.014			
Total	0.3115	17				

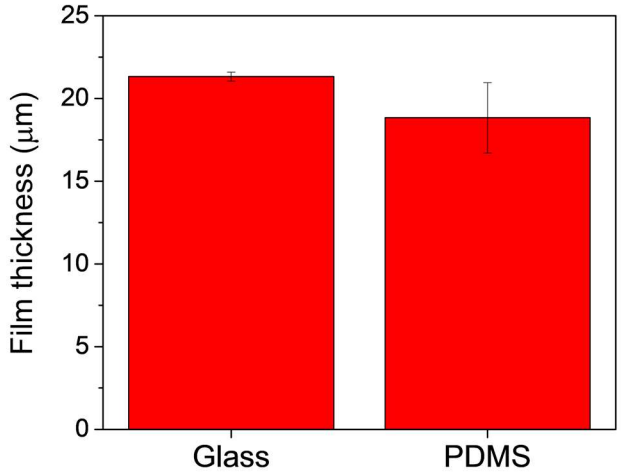

Figure S20. Film thickness of glue molds fabricated using the blade coating method on a glass substrate and on a PDMS substrate.

Table S7: *t*-test comparing the height of glue molds fabricated using the blade coating method on a glass substrate and on a PDMS substrate (C.I. 95%). There is no significant statistical difference between the height of glue molds prepared on a glass substrate or on a PDMS substrate ($t_{calc}<t_{crit}$)

	Glass	*PDMS*
Average	21.321	19
Variance	0.07	5
Number of observations	3	3
Pearson correlation	-0.98881	
Hypothesis test for difference of means	0	
df	2	
t calc	1.801004	
P(T<=t) one-tailed	0.106749	
t crit one-tailed	2.919986	
P(T<=t) two-tailed	0.213499	
t crit two-tailed	4.302653	

Inverse xurography method

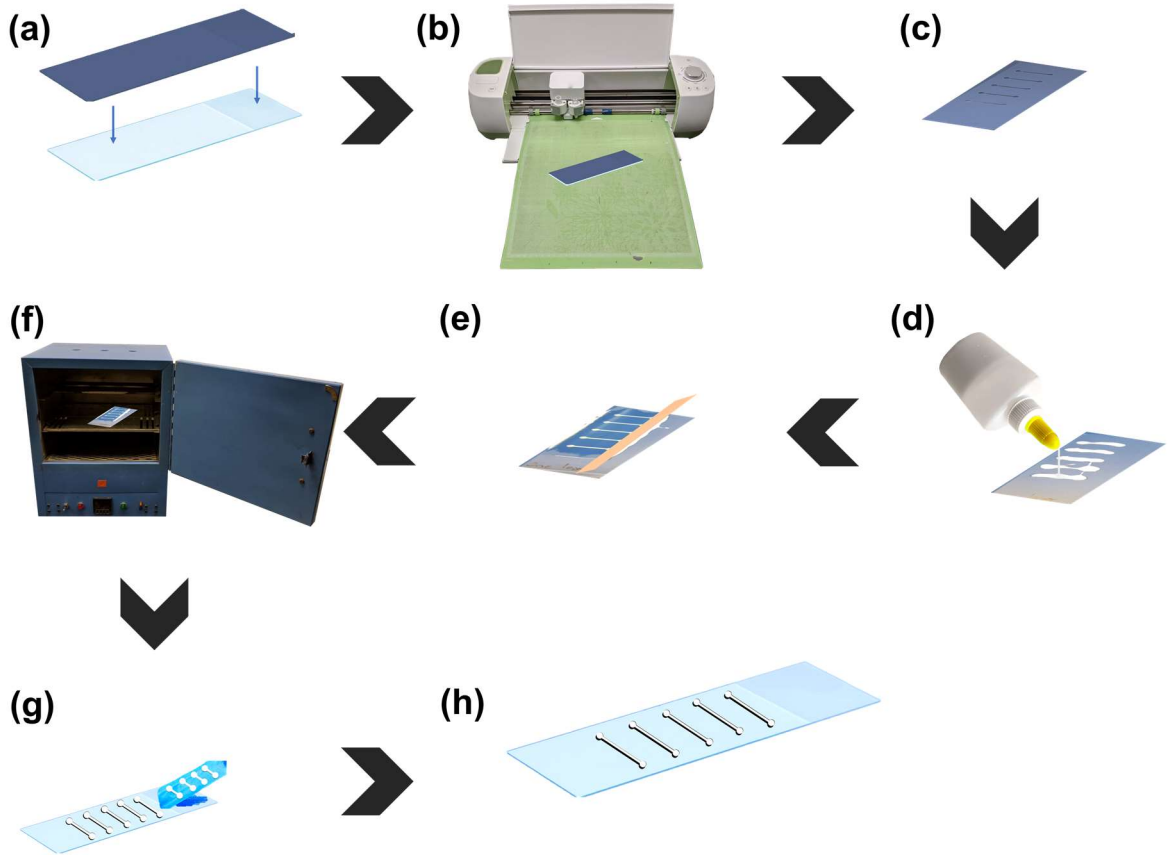

Figure S21. Step-by-step fabrication of PDMS-based microfluidic devices using the inverse xurography method. (a) PVC tape adhesion to a glass backing substrate. (b) CAD designs cutting on tape using a cutting plotter. (c) Removal of the 'internal' molds, leaving the excess of tape on the backing substrate. (d) Water-soluble glue deposition on the cut parts of the mold. (e) Glue spreading onto the mold using a flat edge tool. (f) Glue curing in an oven. (g) Tape removal. (h) Glue mold.

Inverse xurography mold characterization

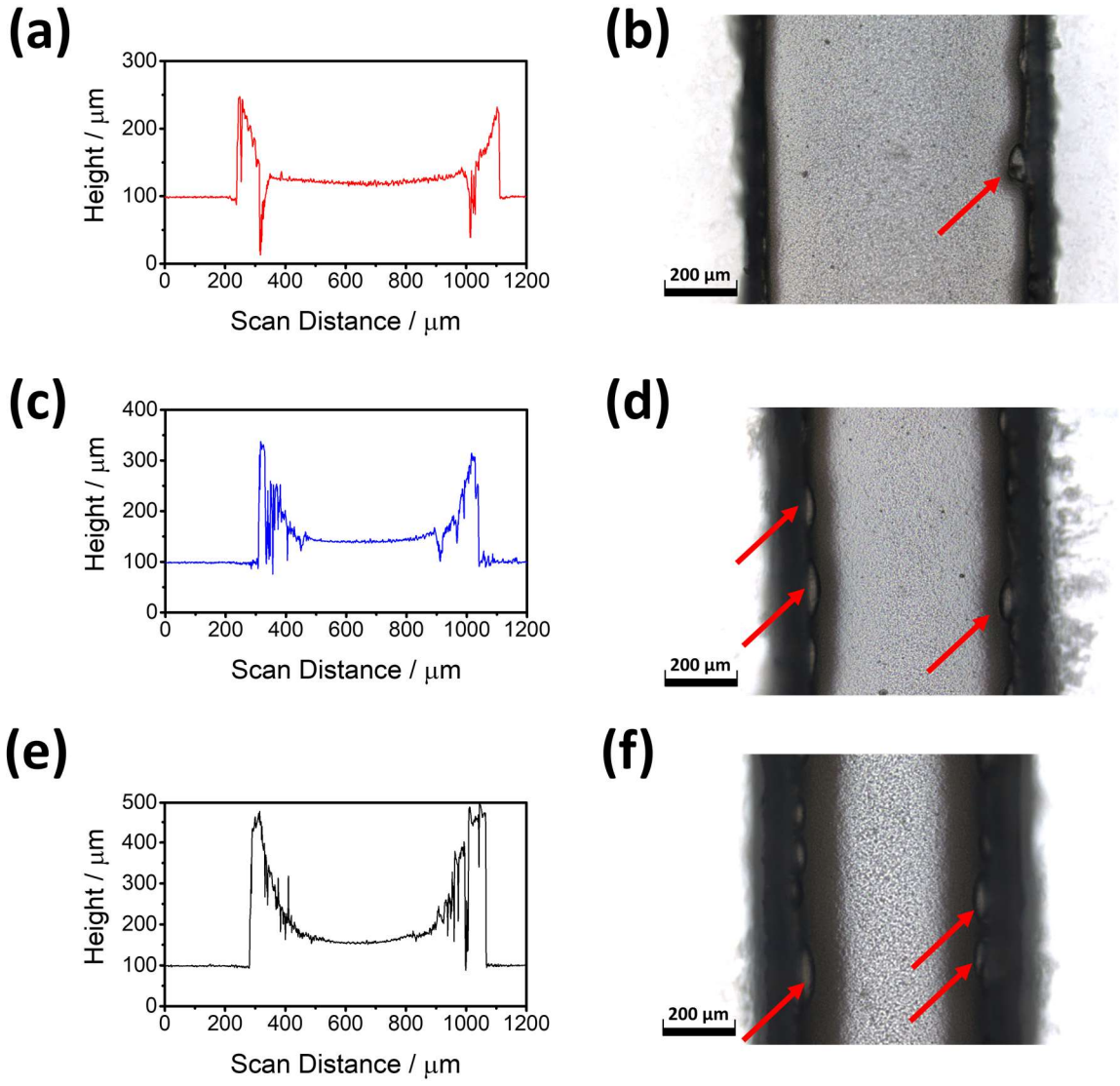

Figure S22. Characterization of glue molds fabricated using the inverse xurography method. (a) Profile of a glue mold fabricated using 1 layer of tape. (b) Laser confocal micrograph of the 1 layer of tape glue mold. (c) Profile of a glue mold fabricated using 2 layers of tape. (d) Laser confocal micrograph of the 2 layers of tape glue mold. (e) Profile of a glue mold fabricated using 3 layers of tape. (f) Laser confocal micrograph of the 3 layers of tape glue mold. The arrows in the micrographs indicate air bubbles entrapped in the glue mold at the tape walls.

Table S8: One-way ANOVA test comparing the surface roughness of molds raster etched using increasing laser speeds (at a constant laser power (12.5%). Raster etched molds using 45% to 70% laser speed did not show a statistically significant difference in surface roughness ($F_{calc}<F_{crit}$)

Raw data					
Surface roughness (root mean square (RMS)) (μm)					
Speed 45%	Speed 50%	Speed 55%	Speed 60%	Speed 65%	Speed 70%
3.069	4.07	4.364	4.563	5.621	3.71
2.879	4.989	4.152	4.692	4.239	3.667
3.976	5.596	4.55	3.664	4.226	4.566

One-way ANOVA – Surface roughness of the raster molds

Source of Variation	*SS*	*df*	*MS*	*F*	*P-value*	*F crit*
Between groups	4.726141	5	0.945228	2.593156	0.081837	3.105875
Within groups	4.374106	12	0.364509			
Total	9.100247	17				

Table S9: One-way ANOVA test comparing the surface roughness of molds raster etched using increasing laser speeds (at a constant laser power (12.5%) and the native glue mold. Raster etched molds using 45% to 70% laser speed showed a statistically significant difference in surface roughness in comparison with the native mold ($F_{calc}>F_{crit}$)

Raw data						
Surface roughness (root mean square (RMS)) (μm)						
Native Film	Speed 45%	Speed 50%	Speed 55%	Speed 60%	Speed 65%	Speed 70%
2.03	3.069	4.07	4.364	4.563	5.621	3.71
2.00	2.879	4.989	4.152	4.692	4.239	3.667
2.059	3.976	5.596	4.55	3.664	4.226	4.566

One-way ANOVA – Surface roughness of the raster molds

Source of Variation	*SS*	*df*	*MS*	*F*	*P-value*	*F crit*
Between groups	17.46204	6	2.91034	9.311287	0.000318	2.847726
Within groups	4.375847	14	0.31256			
Total	21.83789	20				

Table S10: Fabrication costs of glue molds

Material	Quantity	Price ($)	Amount	Cost per device [c] ($)
Elmer's School Glue [2]	3.78 L	27.79	1 mL	0.01
Glass slides [3]	720 slides [a]	367.10	1 [b]	0.51
		Cost per mold		**0.52**

[a] 75 mm by 50 mm.

[b] Can be reused indefinitely, because the molds are water-soluble.

[c] $Cost\ per\ device = \frac{Material\ total\ cost\ x\ Material\ required\ to\ fabricate\ 1\ mold}{Total\ material\ content}$.

Table S11: One-way ANOVA test comparing the height of glue molds after reuse.

Mold heights did not show a statistically significant difference after 3 uses

($F_{calc}<F_{crit}$)

Raw data			
Before	First Cast	Second Cast	Third Cast
Height / µm	Height / µm	Height / µm	Height / µm
23.808	22.421	20.722	23.209
20.841	20.450	22.042	20.310
23.002	23.741	21.316	20.816

One-way ANOVA – Mold reuse - height

Source of Variation	*SS*	*df*	*MS*	*F*	*P-value*	*F crit*
Between groups	3.042	3	1.014	0.511	0.686	4.066
Within groups	15.863	8	1.983			
Total	18.905	11				

Table S12: One-way ANOVA test comparing the channel roughness (as the root-mean-square (rms) of laser confocal profiles) after reuse. The surface roughness of molds did not show a statistically significant difference after 3 uses ($F_{calc}<F_{crit}$)

Raw data			
Before	First Cast	Second Cast	Third Cast
rms / µm	rms / µm	rms / µm	rms / µm
1.721	1.746	1.889	2.253
1.888	2.025	1.832	2.032
1.677	2.06	1.801	1.822

One-way ANOVA – Mold reuse – surface roughness

Source of Variation	*SS*	*df*	*MS*	*F*	*P-value*	*F crit*
Between groups	0.128	3	0.043	1.893	0.209	4.066
Within groups	0.181	8	0.023			
Total	18.905	11				

Hagen-Poiseuille equation

$$R_H = C_{geo}\ \frac{\eta\ L}{A^2} \quad \text{(S2)}$$

R_H is the fluidic resistance of the channel (Pa m^{-3} s);

η is the dynamic viscosity of the fluid (Pa s);

L is the length of the channel (m);

A is the cross-sectional area (m^2);

C_{geo} is the geometric constant of the channel.

For an elliptical channel (which fitted our data better):

$$C_{geo} = \frac{\mathrm{w}(1 + \frac{\mathrm{h}^2}{hw})^2}{h} \quad \text{(S3)}$$

h is the channel height (m);

w is the channel width (m).

Backpressure calculation

$$\Delta P = R_H\ Q \quad \text{(S4)}$$

ΔP is the backpressure (Pa)

R_H is the fluidic resistance of the channel (Pa m^{-3} s);

Q is the fluid flow ($m^3\ s^{-1}$);

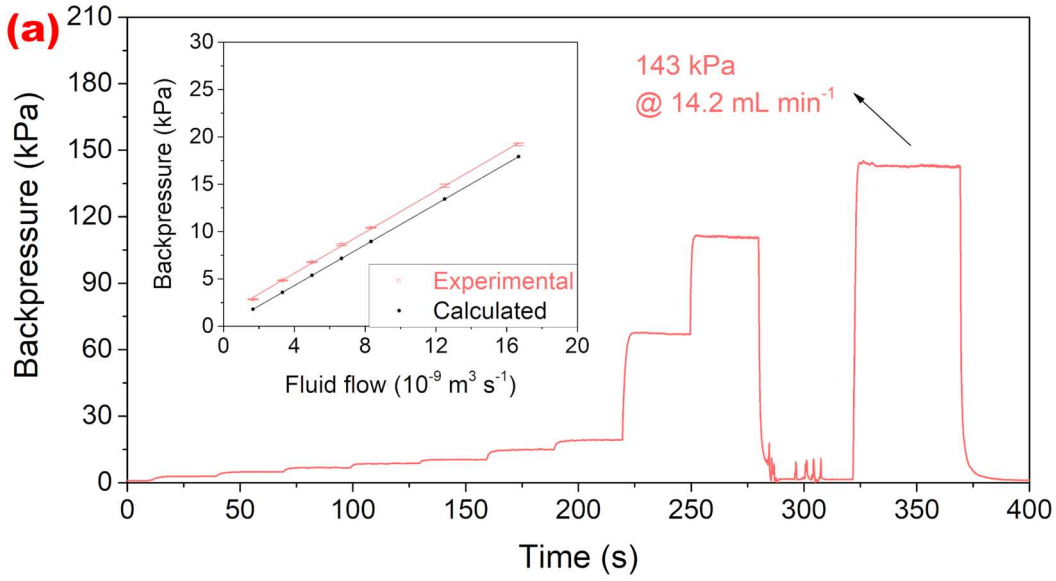
(a)
Backpressure (kPa)
Time (s)
143 kPa
@ 14.2 mL min-1
Backpressure (kPa)
Fluid flow (10-9 m3 s-1)
Experimental
Calculated

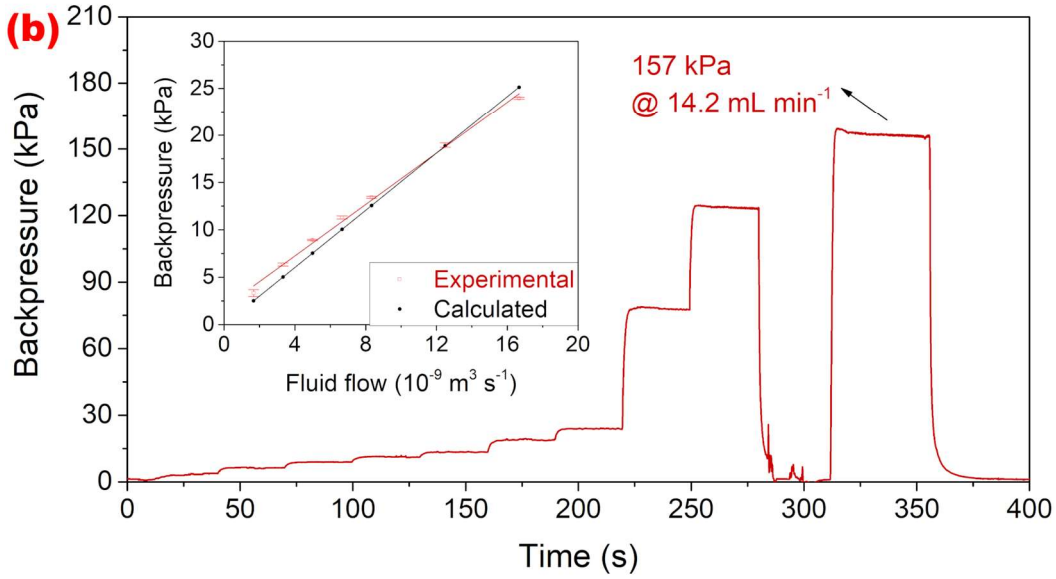
(b)
Backpressure (kPa)
Time (s)
157 kPa
@ 14.2 mL min-1
Backpressure (kPa)
Fluid flow (10-9 m3 s-1)
Experimental
Calculated

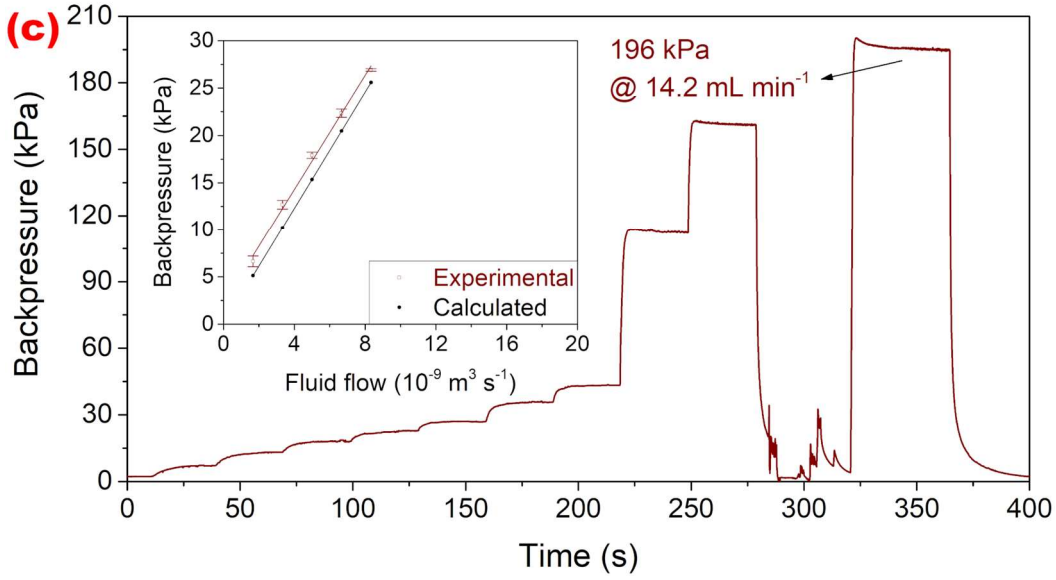
(c)
Backpressure (kPa)
Time (s)
196 kPa
@ 14.2 mL min-1
Backpressure (kPa)
Fluid flow (10-9 m3 s-1)
Experimental
Calculated

Figure S23. Pressure testing of scaffolded PDMS devices. (a) The maximum working pressure registered for this device was 143.0 ± 0.4 kPa (@ 14.2 mL min^{-1}). (b) This device registered a maximum working pressure of 156.7 ± 0.6 kPa (@ 14.2 mL min^{-1}). (c) This device registered a maximum working pressure of 196.1 ± 0.9 kPa (@ 14.2 mL min^{-1}). The region around 300 s in each plot displays noise because the syringe was being refilled with fluid to test the device at the maximum flow of the syringe pump.

The experimental points and the error bars in the inset plots of Figure S23 represent the time average (20 s) and the standard deviation of the backpressure measurements in the main plot, for different fluid flows. Only fluid flows ranging from 100 µL min^{-1} to 1 mL min^{-1} were used to estimate the fluidic resistance for each device, which is the slope of the curves of the inset plots. For device C, the flow range used to estimate the fluidic resistance of the channel was from 100 µL min^{-1} to 500 µL min^{-1}, because elastomeric channels presenting high fluidic resistance deform at higher flow rates, which in turn causes a deviation from linearity of pressure vs. flow plots. It is relevant to point out that none of the devices delaminated during the pressure testing, for the conditions described. The calculated backpressure points were obtained using Equation S4, and the results are summarized on Table S13.

Table S13: Scaffolded PDMS device dimensions and their respective fluidic resistances

Device	Real Width (µm)	Real Height (µm)	Max. Working Pressure (kPa)	Max. Flow (mL min^{-1})	Resistance (10^{12} Pa s m^{-3})	Calculated resistance (10^{12} Pa s m^{-3})
A	439	59	143.0 ± 0.4	14.2	1.09 ± 0.01	1.07
B	449	52	156.7 ± 0.6	14.2	1.36 ± 0.04	1.51
C	430	41	196.1 ± 0.9	14.2	3.0 ± 0.1	3.07
Average[a]	439 ± 9	51 ± 9	170 ± 30	14.2	2 ± 1	2 ± 1

[a] The average row shows the average ± the standard deviation of the measurements for the individual devices

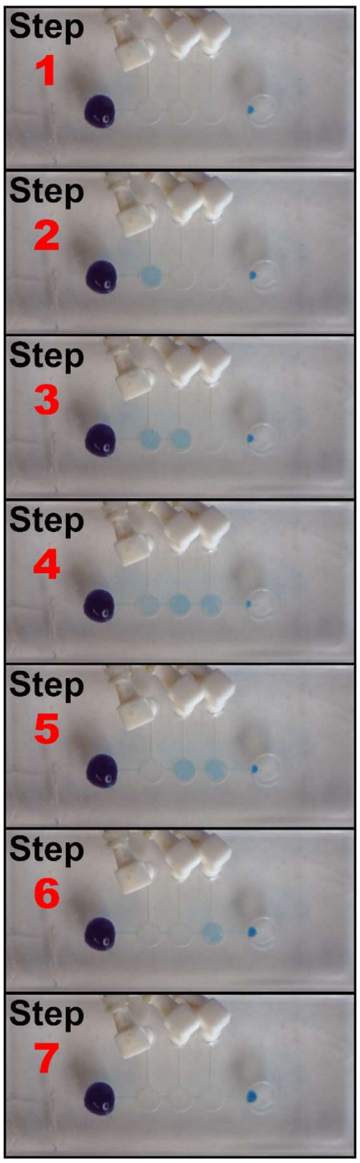

Figure S24. Double chamber pumping routine in a 3-valve normally open pneumatic pump. The valve opening and closing routine is depicted in Figure S8.

SI References

(1) Stockton, A. M.; Mora, M. F.; Cable, M. L.; Willis, P. A. Design Rules and Operational Optimization for Rapid, Contamination-Free Microfluidic Transfer Using Monolithic Membrane Valves. *Sensors Actuators, B Chem.* **2013**, *177*, 668–675.

(2) Staples. Available at: https://www.staples.com/Elmer-s-Liquid-School-Glue-Washable-1-Gallon-1-Count/product_601647 - Access on 04/04/2019.

(3) Sigma-Aldrich. Available at: https://www.sigmaaldrich.com/catalog/product/aldrich/cls294775x50?lang=en&region=US - Access on 04/04/2019.